Influence of the microstructure on fatigue and fracture toughness properties of large heat-treated mold steels

Influence of the microstructure on fatigue and fracture toughness properties of large heat-treated mold steels

D. Firrao[1], P. Matteis[1], P. Russo Spena[2], R. Gerosa[3]

[1]Department of Applied Science and Technology, Politecnico di Torino, P.O.Box 10129 Torino - Italy

donato.firrao@polito.it; paolo.matteis@polito.it

[2]Faculty of Science and Technology, Free University of Bozen-Bolzano, P.O.Box 39100 Bolzano - Italy

pasquale.russospena@unibz.it

[3]Department of Mechanics, Politecnico di Milano, P.O.Box 20133 Milano – Italy

riccardo.gerosa@polimi.it

Abstract

The standard ISO 1.2738 medium-carbon low-alloy steel has long been used to fabricate plastic molds for injection molding of large automotive components, such as bumpers and dashboards. These molds are usually machined from large pre-hardened steel blooms. Due to the bloom size, the heat treatment yields mixed microstructures, continuously varying from surface to core. Negative events (such as microcracks due to improper weld bed deposition or incomplete extraction of already formed plastic objects) or too large thermal/mechanical stresses can conceivably cause mold failure during service due to the low fracture toughness and fatigue resistance typically

encountered in large slack quenched and tempered ISO 1.2738 steel blooms. Alternative steel grades, including both non-standard microalloyed steels, designed for the same production output, and precipitation hardening steels, have recently been proposed by steelworks. However, the fracture toughness and the fatigue properties of these steels, and hence their response during the service, are not well known. Results of an experimental campaign to assess the fracture toughness and fatigue properties, as well as the basic mechanical properties, of a microalloyed and a precipitation hardening plastic mold steel blooms are presented and commented, also in respect to the results previously obtained by two commercial ISO 1.2738 ones. Experimental results show that these steels generally exhibit low fracture toughness values; in the traditional quenched and tempered bloom steels the brittleness may be caused both by the presence of mixed microstructures and by grain boundaries segregation, while in the precipitation hardened one the brittleness probably stems from the grain boundary precipitation phenomena. This study suggests that microalloyed and precipitation hardening steels may be used to produce large plastic mold, yet the fracture toughness still remains the most critical property.

Keywords: plastic mold steels, fracture toughness, fatigue, microstructure, mechanical properties, fractography.

1. Introduction

Large steel molds are employed to manufacture automotive components, such as bumpers and dashboards, by injection molding of reinforced thermoplastic polymers (e.g., polypropylene or ABS). In service, a plastic mold is subjected to the alternate mechanical stresses from die closure and the thermal gradient due to the polymer injection. Mechanical and thermal fatigue (some millions cycles can be required for the production run of one car model) originate. Stresses can be significantly raised by notch effects, defects, and, sometimes, abnormal operations (e.g., incomplete extraction of already formed pieces). Moreover, wear induced by the flow of reinforced polymers may be severe and may be an additional cause for crack nucleation; furthermore, the polymer can infiltrate cracks and acts as a wedge, thus causing fracture propagation.

Plastic molds are commonly machined from large quenched and tempered steel blooms, usually with 1x1 m cross-section and more than 1 m length. The most common standard tool steel grade is the ISO 1.2738, or 40CrMnNiMo8-6-4 [1], although other heat-treatable steels grades may be used. The typical production cycle of these blooms consists of ingot casting, hot forging, and heat treating, Fig. 1. Since the bloom and ingot sections are similar, ingot

inhomogeneities are reduced by repeated hot-forging steps, each consisting of alternated elongation and compression cycles. The bloom heat treatment consists of dehydrogenizing, austenitizing, oil quenching, and tempering, with the heating operations usually performed in air. Depending on their size, dehydrogenization can take a few days, whereas the austenitizing stage (in the range of 840-880 °C) and the tempering stages (in the range of 550-600 °C) may last 1 or 2 days each. The bloom final hardness usually ranges from 300 to 330 HB.

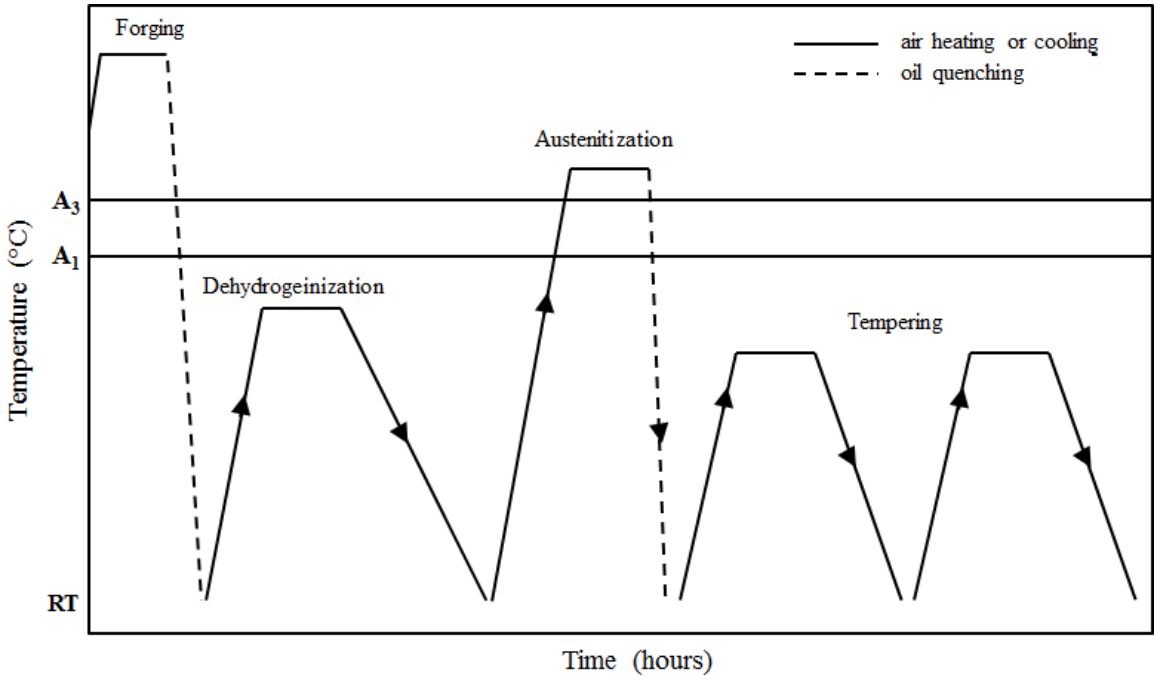

Fig. 1. Schematic illustration of the heat treatment of a large ISO 1.2738 steel bloom. A_3 = upper critical temperature; A_1 = lower critical temperature; RT = room temperature. Diagram not to exact time scale.

After heat treatments the bloom is cut to the required dimension (often asymmetrically) and rough-machined to remove the scale and the decarburized surfaces layer. Blooms for bumper molds are usually sawn to yield a U shape. The mold is machined either by chip removal or by electrical discharge; a final polishing may be required for selected areas. Weld bed deposition operations are often used to correct errors in machining, to allow small changes in design of the plastic component to be injected, and to repair the mold surface (for example to eliminate fatigue or wear cracks originating during the service) to extend the mold life.

During oil quenching, different local cooling rates occur due to the blooms size; thus, after the steelwork heat treatment, the microstructures may vary continuously from the surface to the core of the bloom. Mold machining may be so deep that microstructures occurring at any depth in the bloom can be found at the mold face, yielding a

component with different surface and bulk microstructures, characterized by mechanical properties varying from zone to zone. Previous studies [2, 3] have assessed the deleterious influence of these slack quench mixed microstructures upon the toughness of large quenched and tempered ISO 1.2738 steel plastic molds. To date, toughness enhancements in these steel components are mainly pursued through the use of alternative proprietary steels with the aim either of yielding more uniform microstructures and better mechanical properties throughout the mold section, or of improving weldability (often by using a carbon content lower than 0.3 %). These steels include microalloyed medium carbon steels and precipitation hardenable ones. In respect to the traditional ISO 1.2738 steel, microalloyed steel grades display small additions of elements, such as vanadium, niobium, and titanium, to increase yield and tensile strength by precipitation strengthening and grain refinement [4]. Moreover, microalloyed steels are designed with a lower carbon content (0.25–0.30 %) to improve steel weldability; alloy elements such as molybdenum, chromium, and boron are generally needed to keep strength and hardenability similar to the ISO 1.2738 steel.

Precipitation hardening steel grades undergo a solution heat treatment followed by age-hardening to improve their strength and hardness properties by precipitation of second phases. The P21 [5,6] standard grade steel, for example, contains 0.2% C, 4% Ni, 1.2% Co, and lower amounts of V, Al, Mn, Si, Cr [5]; yet, most grades are proprietary and not disclosed in detail [7]. The solubilization temperature can be subcritical, as for the P21 grade (albeit after an hypercritical annealing) [5,8], or hypercritical, for some proprietary grades, whereas the aging temperature is always subcritical (e.g., 530 °C for the P21 grade [5,8]), and therefore yields very limited dimensional variations. The final hardness is usually in the 37-42 HRC range [7], depending on the temperature and time used in the age-hardening heat-treatment. Precipitation hardening can be done after machining, since it causes only limited deformations [9], and may yield more homogeneous microstructures and mechanical properties throughout the bloom sections in large molds with complex shapes. Furthermore, in some cases (e.g., for the here proposed steel), the preliminary heat-treatment performed on the as-forged bloom can employ air cooling after austenitization, as opposed to oil quenching in the case of traditional hardened steels, thus yielding much lower temperature gradients and minimizing residual stresses.

Also for precipitation hardening and microalloyed medium carbon steels fracture toughness and fatigue properties are not well known. Therefore, in the present work experimental results concerning the fracture toughness and fatigue properties, as well as hardness, tensile, and resilience obtained from samples cut from a microalloyed steel

bloom or from a precipitation hardening steel one are reported. Mechanical properties are compared with those obtained by the authors in previous studies carried out on two commercial ISO 1.2738 steel blooms used to fabricate large plastic molds [2, 3], interpreting differences on the basis of the different microstructures occurring inside the blooms. Furthermore, some samples cut from an examined ISO1.2738 steel bloom and the precipitation hardening one were re-heat-treated in a laboratory furnace for three purposes: i) to investigate the effects of the austenitization duration; ii) to investigate whether the steel mechanical properties are influenced by the location in the bloom due to the different thermal history occurring throughout the bloom during the final heat treatment (for the ISO 1.2738 steel bloom); iii) to evaluate the influence of age-hardening heat treatment on the mechanical properties and microstructures of the precipitation hardening steel.

2. Materials, sampling and experimental methods

Two quenched and tempered ISO 1.2738 steel blooms produced by different steelmakers (herein indicated with the letter A, and B), a microalloyed quenched and tempered (C) and a precipitation hardening (D) steel bloom were selected for this work. The chemical compositions were measured by optical emission spectrometry and are listed in Tab. I. In respect to the ISO 1.2738 steel blooms, the microalloyed one displays lower carbon and higher molybdenum content, as well as the presence of small amounts of boron, niobium, and zirconium. Vanadium is present in all the examined blooms in order to prevent excessive grain coarsening during the long steelwork heat treatments.

Tab. I. Compositional limits (wt.%) for the plastic mold steel grade ISO 1.2738, chemical analysis of the examined 1.2738 blooms A and B, microalloyed quenched and tempered bloom C, and precipitation hardening bloom D.

Class	Grade	C	Mn	Cr	Ni	Mo	Si	Nb	V	B	Zr	S	P
QT*	ISO 1.2738	0.35 0.45	1.3 1.6	1.8 2.1	0.9 1.2	0.15 0.25	0.2 0.4	n.r.	n.r.	n.r.	n.r.	0 0.03	0 0.03
	A	0.39	1.5	2.1	1.0	0.20	0.22	n.d.	0.02	n.d.	n.m.	0.009	0.011
	B	0.42	1.5	2.0	1.1	0.21	0.37	n.d.	0.08	n.d.	n.m.	0.002	0.006
	C	0.28	1.6	1.4	1.1	0.60	0.28	0.02	0.12	0.0013	0.03†	<0.001	0.007
PH**	D	0.16	0.7	0.2	3.2	3.2	0.22	n.d.	0.08	n.d.	n.m.	0.002	0.005

*QT: quenching and tempering, **PH: precipitation hardening,

[†]Estimated, n.r.: not restricted, n.m.: not measured, n.d.: not detected.

The production process used to fabricate all blooms is similar to that shown in Fig. 1. Nevertheless, the D bloom was also subjected to an additional hypercritical heat treatment between the forging operations and the final heat treatment. The blooms' recorded or estimated forged size and final steelwork heat-treatment temperatures are shown in Tab. II. The L direction defines the maximum length of the ingot casting and the direction of largest deformation during forging, whereas the orthogonal directions S and T are equivalent.

Tab. II. Forged size and final steelwork bloom quenching and tempering heat-treatments.

Bloom	Bloom size (mm)			Austenitizing		Cooling Medium	Tempering temp. (°C)	
	L	T	S	temp. (°C)	grain (µm)		1st	2nd
A	2240*	900*	900*	860*	10 - 100†	air*	600*	600*
B	2970	1285	1190	850	10	Oil	590	550
C	2900	1260	1020	950	265	Water	590	550
D	2400	1500	500	1020	130	Air	400	400

[*]Estimated from delivered size, test results and/or common usage, [†]Inhomogeneous.

The A, B, and C blooms were cut to a U shape to fabricate bumper molds, Fig. 2; the residuals were used to fabricate series of samples at increasing depth from the surface to the core of the blooms, being representative of the different thermal histories occurring during the production process. In most cases, the test samples were cut with orientation L (for tensile and rotating bending fatigue tests) or LT (for Charpy, fracture toughness, and fatigue crack growth tests), at increasing depth along lines in direction T (A, and B blooms) or S (C bloom), passing as close as possible to the bloom core, Fig. 2. However, the D bloom samples were obtained at a 170 mm depth only. The depth of a sample is defined as the distance between the examined portion of the sample itself (e.g., the fracture initiation zone of a large fracture toughness specimen) and the nearest forged and heat treated surface in the sampling direction (direction S for C bloom, and T for A and B blooms).

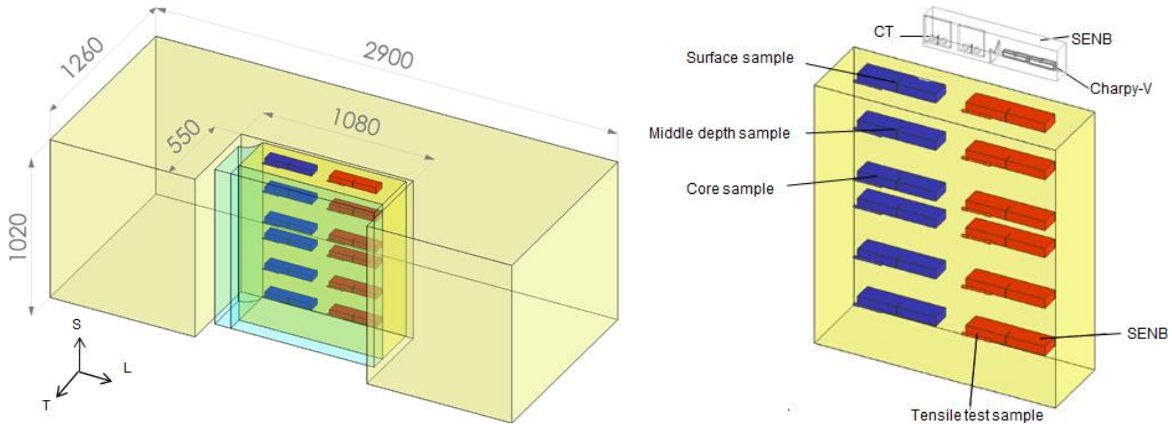

Fig. 2. Example of bloom sampling: original positions of the C bloom specimens.

Some samples, cut from the B and D bloom steels were re-heat-treated in a laboratory furnace; they are here called "RHT" samples. The B bloom samples were re-austenitized in the 850 to 870 °C range for about 45 minutes, and then either isothermally treated at 600 °C or fully quenched in nitrogen gas (cooling rate between 2.5 and 12.5 C/s in the range of 700-500 °C) and tempered in two stages at 595 and 555 °C for about 150 minutes each (similar to those adopted in steelwork). During the heating stages vacuum or protective gases were employed to prevent scale and surface decarburization; a quenching media less severe than those used in the industry was used to minimize quenching distortions, since some specimens were machined before the heat treatment. During the re-heat-treatments, the D bloom specimens were re-austenitized at 1050 °C, air cooled, and tempered twice at 400 °C (these temperatures are similar to those adopted in steelwork). Then, both as-received and RHT D bloom samples were age-hardened in air at 470, 510 or 550 °C up to 8 h; specimens were extracted from the furnace at several step to build age-hardening curves.

The microstructures were examined by both optical and scanning electron microscopy, after mechanical polishing and chemical etching by Nital. The prior austenite grain size was measured with the three-circle intercept-count method [10] after Bechet-Beaujard etching [11].

The mechanical tests were performed at room temperature, according to the ISO and ASTM standards, unless otherwise specified. The fracture toughness (K_{Ic}) tests [12-14] were performed on single-edge notched beam (SENB) samples with 35 or 38 mm thickness cut from B and C blooms, both with LT orientation (in respect to the original blooms), as well as on similar RHT, quenched and tempered B bloom samples, and on one D specimen aged for 3.5 h at 525 °C.

Fatigue Crack Growth (FCG) tests [15,17] were performed on 6 mm thick compact tension (CT) samples or 12.5 mm thick SENB samples, both with LT orientation, with 40 Hz sinusoidal waveform, load control, and constant load ratio R = 0.1.

The CT samples crack length was measured optically on both polished sample surfaces, the fatigue test being interrupted to perform each measurement; crack-length differences between the two sides in excess of 25% of the thickness occurred at times in the low ΔK range (ΔK being the cyclic amplitude of the stress intensity factor, SIF). The crack length of SENB samples was monitored continuously by using a compliance method on load-crack opening displacement (COD) measures, and recorded at fixed crack length intervals. The secant method and the incremental polynomial method (of order 2) were used to analyze the ΔK-decreasing (with load-shedding K-decreasing procedure) and ΔK-increasing (with constant-load-amplitude procedure) datasets [15], respectively.

Charpy V-notch impact tests were performed on two series of B steel samples, cut close to the surface and the core of bloom, respectively. The temperature of the Charpy test ranged from 20 to 325 °C.

Series of rotating bending fatigue stress-life (S-N) tests were performed with 50 Hz frequency according to the staircase method on hourglass samples with 6 mm minimum diameter. The endurance limit was defined as the stress corresponding to a 50% survival probabilities at $4.2 \cdot 10^6$ cycles (proportionate to an average automotive production run).

3. Materials, sampling and experimental methods

3. 1 Microstructures

The prior austenitic grains (PAG) size resulting from the industrial heat-treatment of the blooms is shown in Tab. II. The PAG size of the A and B blooms ranges from 10 to 100 μm, probably because of their different vanadium content (vanadium carbides can pin austenite grain boundaries at high temperature) used for this steel. The A bloom exhibits an inhomogeneous and almost bimodal distribution, with adjacent regions with grain size ranging from 10 to 100 μm; therefore, it was not possible to measure a reasonable average value. By contrast, the B bloom has a quite homogeneous grain size, both at surface and core. The PAG size of the C and D blooms is larger, despite they have larger vanadium content, likely because the vanadium carbides dissolve at the higher austenitization temperatures used during the industrial heat-treatment of these steels. In fact, some austenitizing tests carried out by the authors in a previous study [16] have demonstrated that the PAG size of the C steel was only ~20 μm after

heating at 885 °C, that is just below the estimated vanadium carbides dissolution temperature for this steel [17].

The varying microstructures of the blooms were examined at increasing depth along either the S direction (C bloom) or T direction (A and B blooms), from surface to core, the large bloom size implying local cooling rates, during the quenching, sensibly different as a function of the depth. The microstructure of the ISO 1.2738 steel blooms, Fig. 3, consists mainly of tempered martensite close to the surface, of lower and upper bainite (affected by tempering) in most of the bloom volume, and of fine and ultra-fine pearlite at core (the lamellar morphology was resolved by SEM, as for instance shown in Fig. 4); rare islands of retained austenite are also detected in the bloom section. The tempered martensite and the lower bainite have a needle-like appearance, whereas, going towards the bloom core, the microstructural constituents become less acicular and pearlite colonies appear and become increasingly common at larger depth. It can be noted that the microstructures are generally finer in the B bloom than in the A one, probably due to smaller PAGs.

Bloom	Surface	Core
A	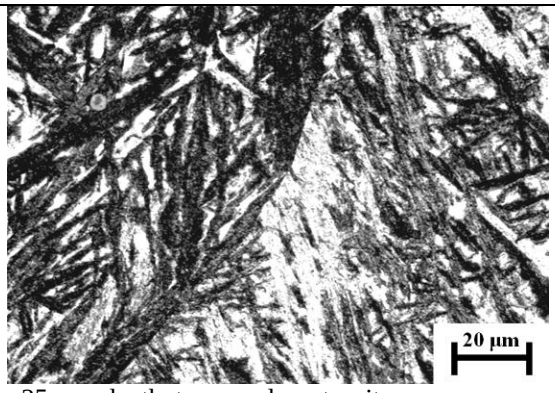 ~25 mm depth, tempered martensite	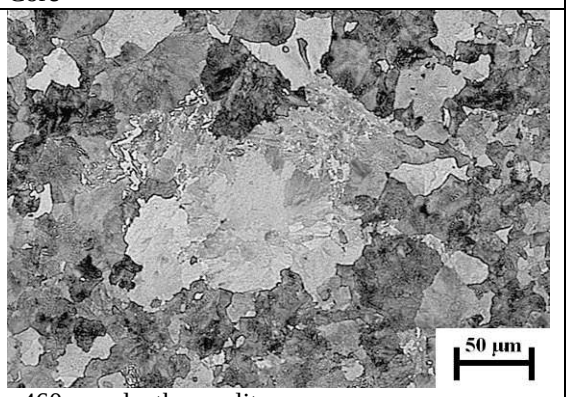 ~460 mm depth, pearlite
B	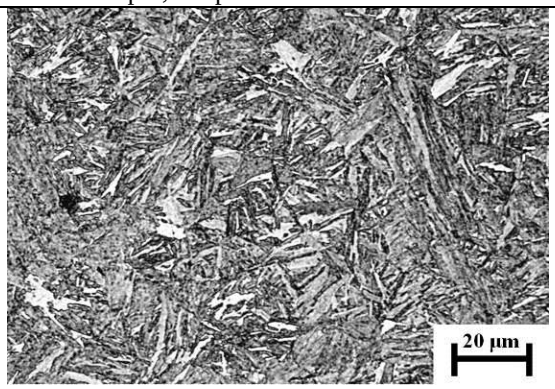 ~55 mm depth, tempered martensite	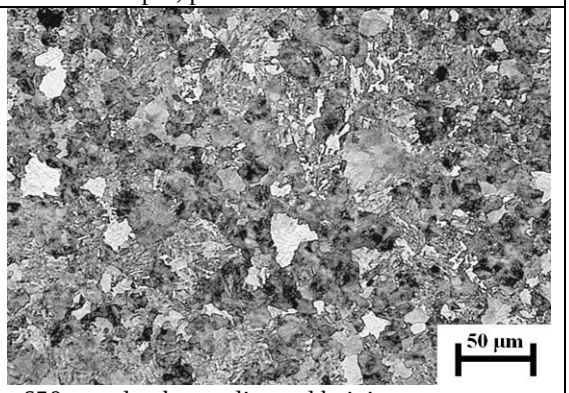 ~650 mm depth, pearlite and bainite

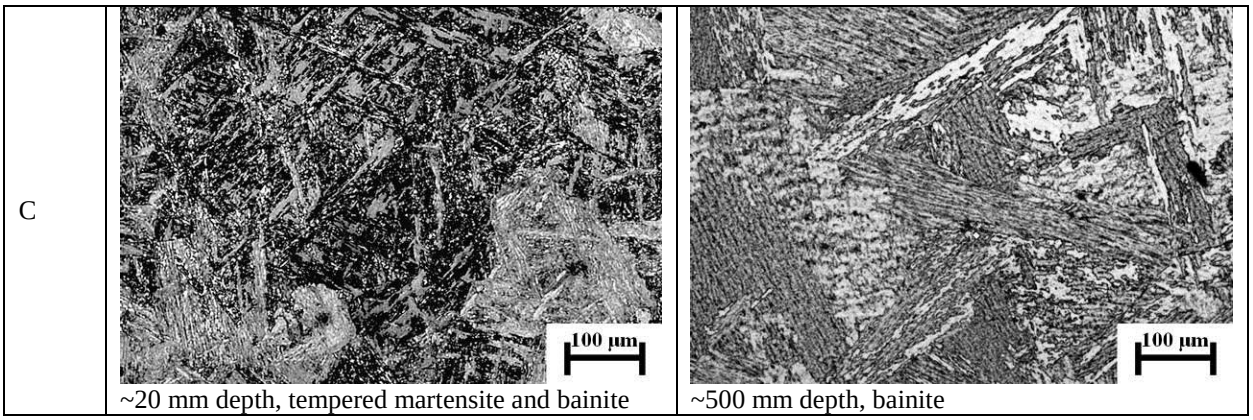

Fig. 3. Surface and core microstructures of the A, B, and C blooms. Optical microscopy.

In A bloom, pearlite first appears at a smaller depth than in B bloom, 155 mm and 285 mm respectively, and with a less homogeneous distribution (i.e. mainly at PAG boundaries). Close to the core, fine pearlite, is the main constituent in all examined blooms; nevertheless a significant fraction of bainite is still detected in B bloom, Fig. 4, whereas the same constituent is almost absent in A bloom.

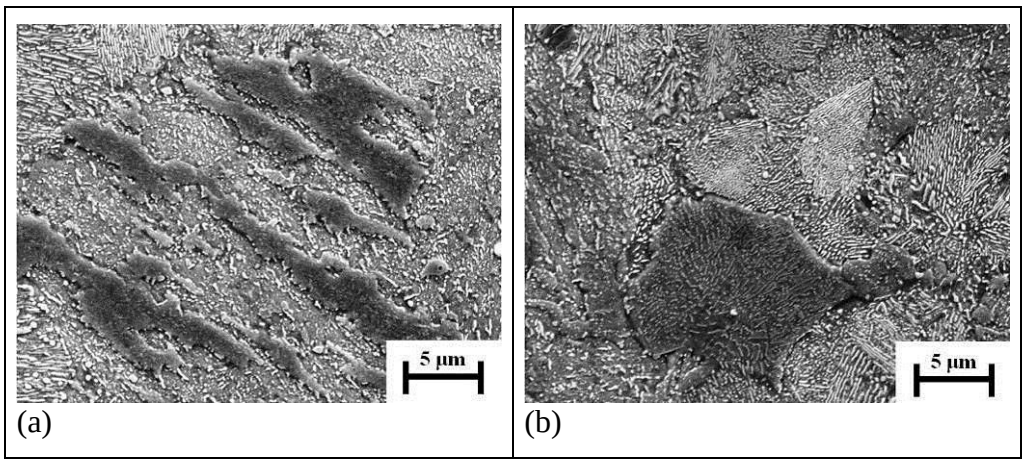

Fig. 4. SEM details of metallographic constituents at core (650 mm depth) in B bloom: upper bainite modified by tempering (a) and fine pearlite (b).

The microstructure of the C bloom is quite homogeneous in the whole section of the bloom. The steel shows an acicular microstructure mainly consisting of tempered martensite mixed with bainite (affected by tempering). The microstructure coarsens at increasing depth and the tempered martensite is gradually replaced by bainite packets.

The microstructures of the ISO 1.2738 RHT specimens depend on the laboratory heat treatment: the quenched and tempered specimens had a fully tempered martensite microstructure, whereas the specimens isothermally treated at

600 °C had a pearlitic microstructure. Fully tempered martensite or pearlite can be compared to the similar microstructures present at the surface and at the core of an ISO 1.2738 steel bloom.

The microstructure of the examined part of D bloom is temper-modified bainite, Fig. 5a,b, whereas the laboratory RHT samples consist mainly of tempered martensite, with some temper-modified bainite, Fig. 5c. No modifications due to aging are detected in the bloom material by optical microscopy, whereas the RHT material after aging generally exhibits a coarser carbide distribution and more evident PAG boundaries than before aging, Figs. 5d, e, f.

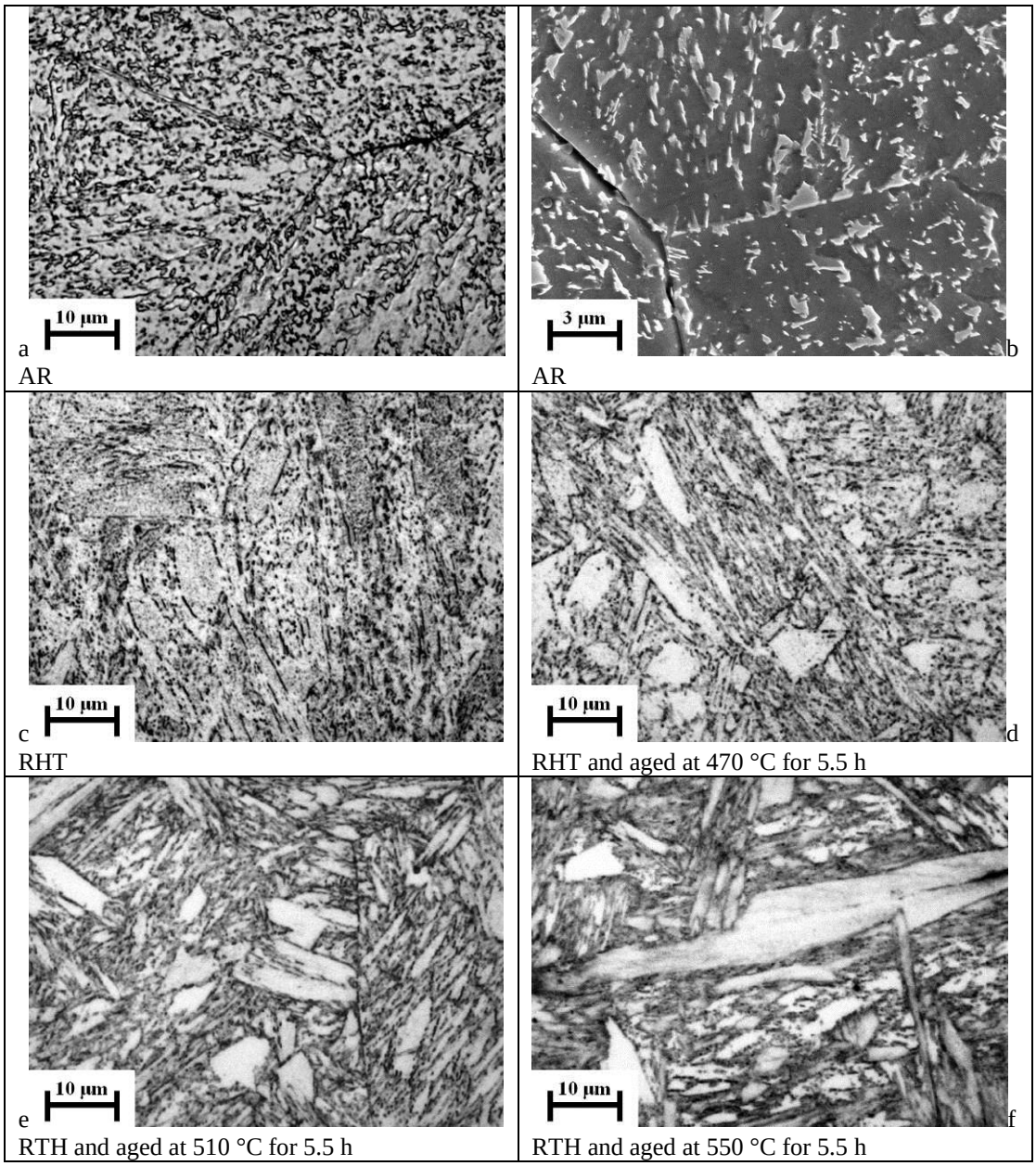

Fig. 5. Microstructure of the D bloom in as-received and RHT. RHT = austenitizing at 1050 °C, water quenching,

and double tempering at 400 °C.

3.2 Mechanical properties

Hardness and tensile tests were performed both on the as-received specimens, obtained at increasing bloom depths, and on the RHT ones. In particular, the tensile specimens were oriented along the L direction, while hardness tests were performed on ST plane. The tensile and hardness test results are shown in Fig. 6. Consistently with the microstructures, the tensile and hardness properties of the ISO 1.2738 steel blooms are significantly influenced by bloom depth. The hardness of B bloom significantly decreases from surface to 200 mm depth and may be related to the transition from tempered martensite to tempered bainite microstructure; the successive hardness plateau between 200 and 540 mm depth approximately corresponds to the mainly tempered bainite microstructures; finally, the minimum value at core is clearly related to the appearance of the pearlite; lower core values are found along the test line closes to the bloom three-dimensional center point (Fig. 6, test line II), than along the other one (Fig. 6, test line I). The diagram of the tensile properties (which were measured along test line I only), has a profile similar to the corresponding hardness curve, showing a similar decrease at core. On the contrary, the hardness of the A bloom increases from surface to mid-depth achieving the maximum hardness at about 200 mm of depth, and then presents a sharp decrease at core; the reason of this behavior is not evident, but it may be attributed to a short duration of the tempering stage of the steelwork heat treatment and/or to elemental segregations (a concentration gradient from surface to core was detected by optical emission spectroscopy for several alloying elements [18, 19]). The diagram of the ultimate tensile strength follow a pattern similar to the corresponding hardness curve, showing a sharp decrease at core and shallow maximum at about 250 mm depth; whereas the yield stress presents first a slight continuous decrease with depth, followed by a steep descent to the minimum at core. In all cases, the hardness and tensile profiles for each steel are almost symmetrical in respect to the centerline of the bloom.

Consistently with the more homogeneous microstructures, the hardness and tensile tests on the C bloom yielded comparable values at all depths inside the bloom compared to the A and B ones. Hardness, yield strength (YS), and ultimate tensile strength (UTS) are almost constant and close to 375 HV 100, 990 MPa, and 1145 MPa, respectively.

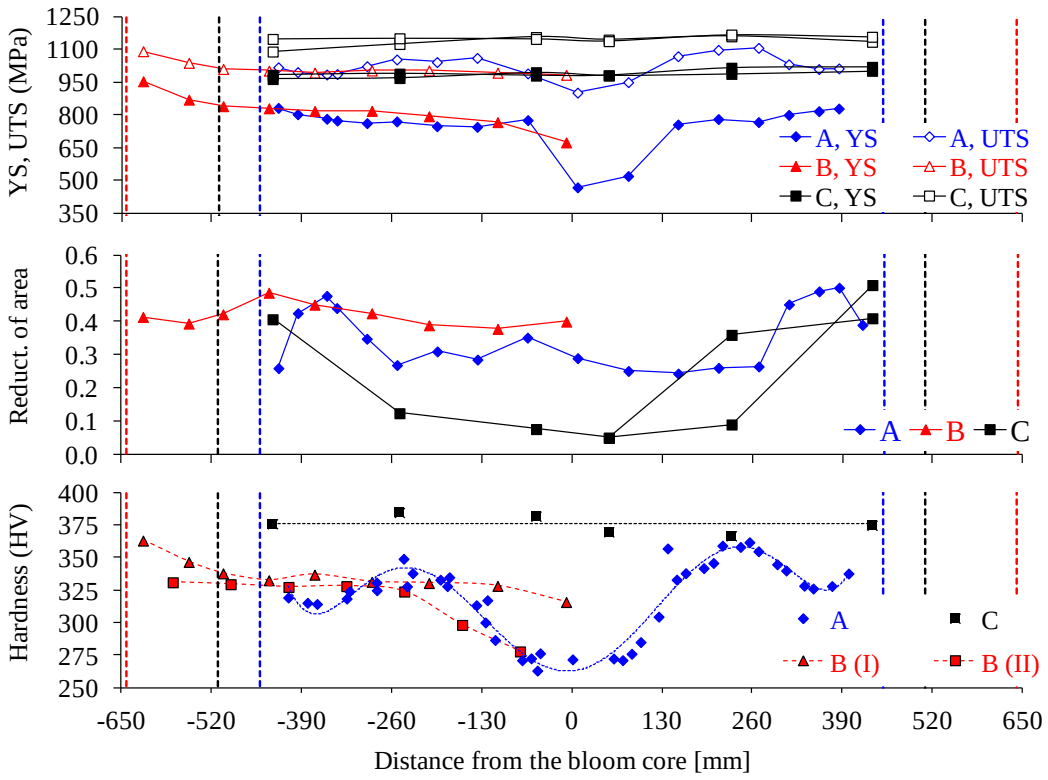

Fig. 6. UTS, YS, reduction of area, and HV 100 hardness of the A, B, and C blooms. Shaded lines represent the blooms core and surface (refer to Tab. II). Hardness tests performed in the B bloom along two parallel lines (I and II). Some A bloom HV hardness values were converted from HRC ones.

The examined portion of D bloom has a hardness, YS, and UTS of 380 HV 100, 850 MPa, and 1150 MPa, respectively. The age hardening of D steel, both in as-received the in RHT conditions, is generally complete after ~1.5 h; the maximum hardness is almost constant for aging durations up to 8 h, a possible light overaging is only detected for RHT specimens aged at 550 °C, Fig. 7. Agings at increasing temperatures yield larger hardness, YS, and UTS values, but decreasing uniform elongation and total elongation (at fracture). Aged as-received and aged RHT samples have different uniform elongation, YS, and UTS for the same aging temperature, but these differences decrease at increasing aging temperature, Fig. 8. On the contrary, the difference in total elongation increases, in particular, aged as-received tensile samples fail without appreciable necking.

The amount of carbides detected by SEM [20] generally decreases with increasing the aging duration and temperature (both for as-received and RHT materials). It is thought that the carbides formed during prior steelwork heat treatments are unstable at the aging temperature and dissolve, while undetected finer carbides, possibly with

different compositions, are re-precipitated, thus causing the strengthening effects.

The second phases electrochemically extracted from the RHT sample and aged at 550 °C for 7 h showed XRD diffraction peaks referable to η-MoC, and possibly to V_7C_8 [20]. The EDS analysis of the same second phases performed on compacted powder confirmed the occurrence of molybdenum and of lower amounts of vanadium, iron, chromium, and silicon. Hence, it is thought that η-MoC and possibly V_7C_8 are among the abovementioned carbides responsible for the age hardening of the D steel.

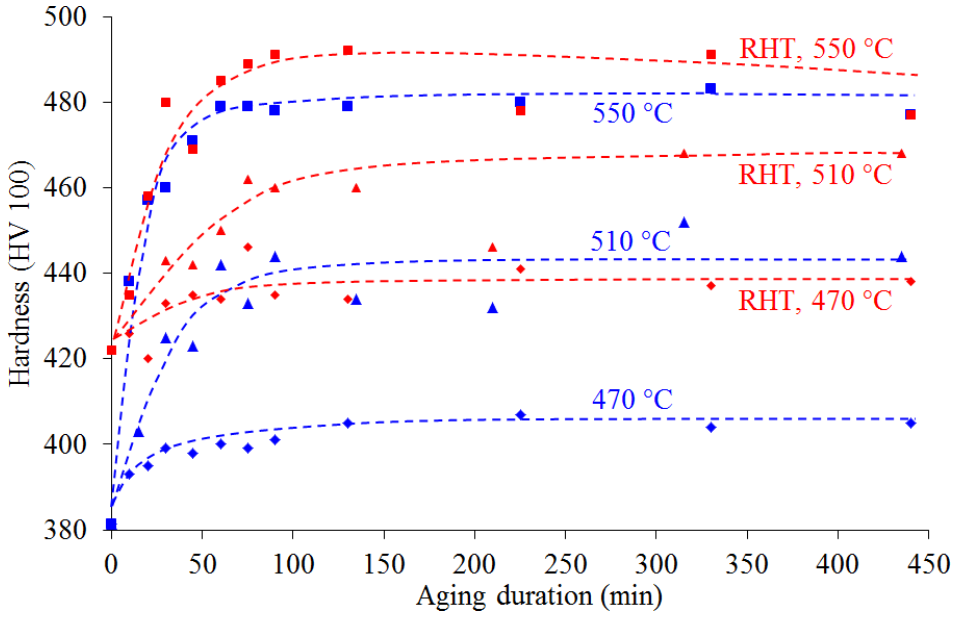

Fig. 7. Age-hardening curves obtained by D bloom specimens in the as-received and RHT conditions. Aging temperature: 470, 510, and 550 °C.

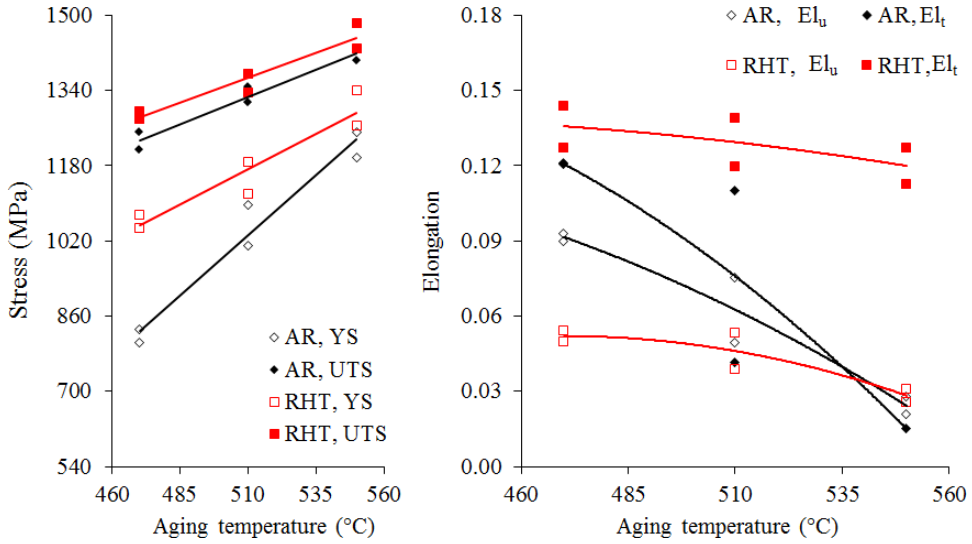

Fig. 8. Tensile properties of the D bloom specimens in as-received (AR) and RHT conditions after aging heat treatment, duration 2.5 h. EL_u = uniform elongation; El_t = total elongation.

In most K_{Ic} specimens, a pop-in occurred before the maximum load. The curves of force versus crack opening displacement do not show any significant plastic (not linear) contribution and the lateral shear lips are very small.

The B bloom fracture toughness is quite low, ranging from ~35 MPa√m at surface to ~45 MPa√m at core; the C bloom fracture toughness is ~55 MPa√m close to surface, but somewhat lower at mid-depth and core (~40 MPa√m), Fig. 9. The RHT B bloom specimens exhibit a much higher fracture toughness than original as-received ones, even if the former show a large scatter (86, 68, 103, 62 MPa√m). The average fracture toughness of the D bloom is 70 MPa√m, but it decreases to 44 MPa√m (mean of four tests) after the aging treatment at 525 °C for 3.5 h. The lower toughness of the C bloom specimens cut from mid-depth and core regions, compared with those of the surface region, is also highlighted by the much lower tensile reduction of area (Fig. 6), and by the lack of detectable necking in the core tensile samples.

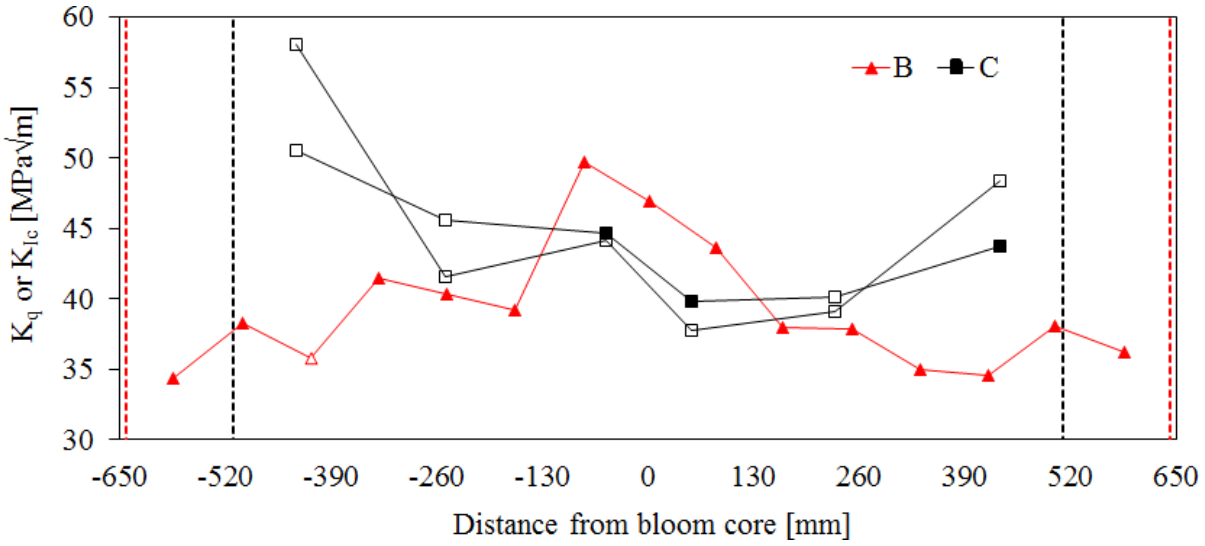

Fig. 9. Fracture toughness of the B and C bloom specimens, as a function of the original depth (two series of samples were cut from two parallel lines, throughout the C bloom). Shaded lines represent the blooms surfaces. The empty symbols represent measurements having $P_{max}/P_q > 1.10$ [13].

The room temperature impact energy (KV) of B bloom is ~10 J both for core and surface specimens, whereas RHT specimens exhibit somewhat improved values (~20 J), Fig. 10a. The fracture appearance transition temperature (50% FATT) is ~270 °C for the material close to the bloom surface and ~150 °C for that close to core.

Further Charpy measures were performed at 175±2 °C with the aim of testing, both the A and B blooms, close to the polymer injection temperature, and between the aforementioned transition temperatures, Fig. 10b. The 175 °C impact energy of B bloom increases with depth and coherently to the surface and core transition curves. The impact energy values of A bloom are higher than those of B bloom at the same temperature, but they have an opposite (decreasing) trend in respect to depth. The latter result could be caused by an increasing concentration of alloying elements, from surface to core, due to the segregation effect occurred during the ingot casting and not eliminated by the following forging procedure.

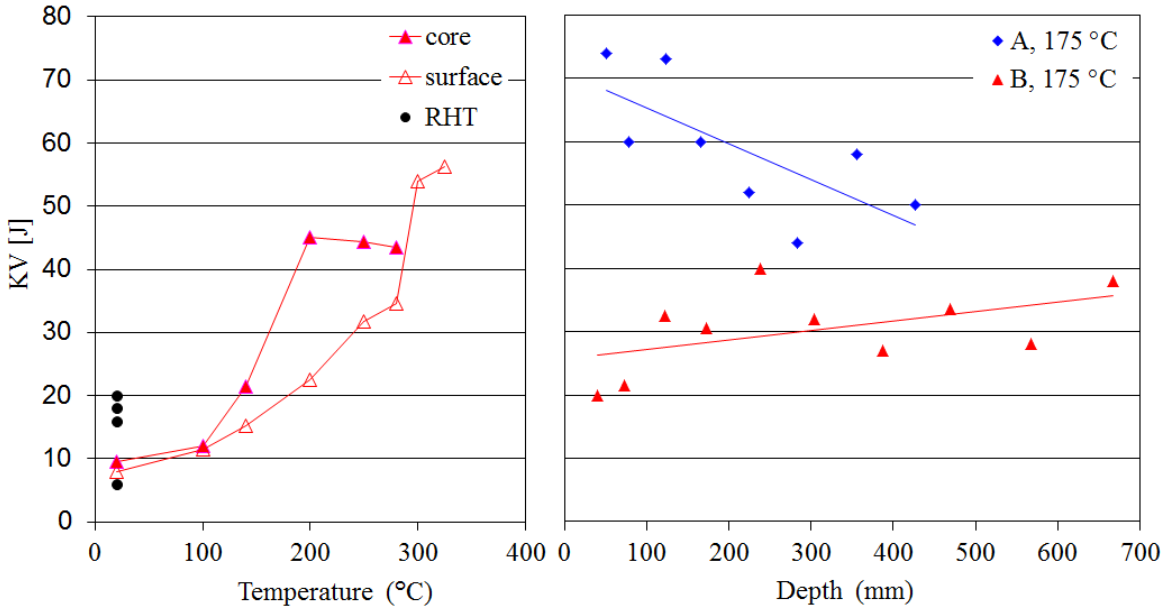

(a) (b)

Fig. 10. Charpy test results. (a) Charpy ductile-to-brittle transition curves of the as-received B bloom specimens(surface and core position), also including Charpy value of RTH specimens at room temperature; (b) 175 °C impact energy of A and B blooms from surface to core depth.

3.3 Fatigue

The fatigue crack growth rates (regardless of the measurement techniques) of B and C steels at different bloom depth, with the former both in the original and in the RHT condition, are herein stated. Results are expressed in terms of crack tip stress intensity factor range (ΔK), from the fatigue threshold to the Kmax controlled instability (i.e. fracture). The ΔK threshold value was determined by the decreasing method down to crack growth rates of about 10^{-10} m/cycle. The overall FCG behavior of the as-received B and C bloom samples are shown in Fig. 11. The Paris slope of B bloom sample ranges from 2.4 to 3.2, whereas that of the C one is slightly steeper. In this way, even if the C bloom samples exhibit a lower FCG rates at stress intensity factor ranging up to about 15 MPa√m, their FCG rates exceed those of the B bloom samples at ΔK values higher than 20 MPa√m. The ΔK threshold of all samples were estimated between 5 and 6 MPa√m, even though the data dispersion could hide possible differences in the FCG threshold region.

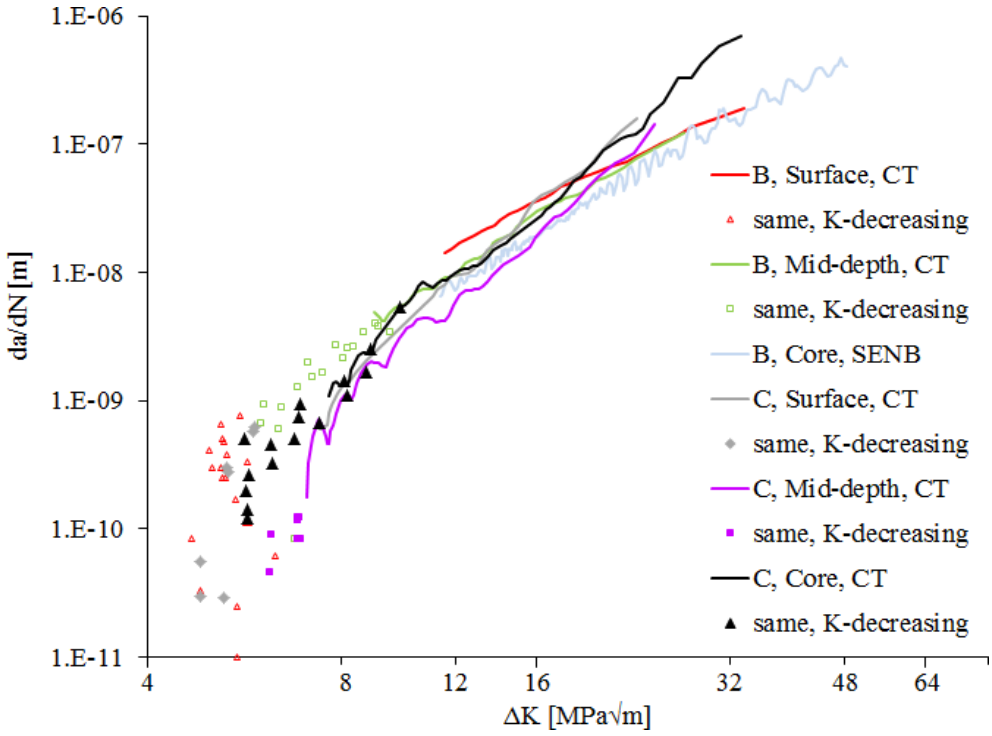

Fig. 11. FCG behavior of steel B and C bloom specimens at different bloom depth. Plot of K-increasing (lines) or K-decreasing (isolated points) tests. SENB or CT samples.

The results of the fatigue tests performed on B bloom samples in as-received and RHT conditions are in Fig. 12. The FCG rates of the tempered martensite sample is similar to that of the bloom microstructures (although the former interrupts at a higher ΔK due to the higher K_{Ic}). The pearlite sample exhibits a similar Paris slope in the linear range, but slower FCG than the core bloom sample.

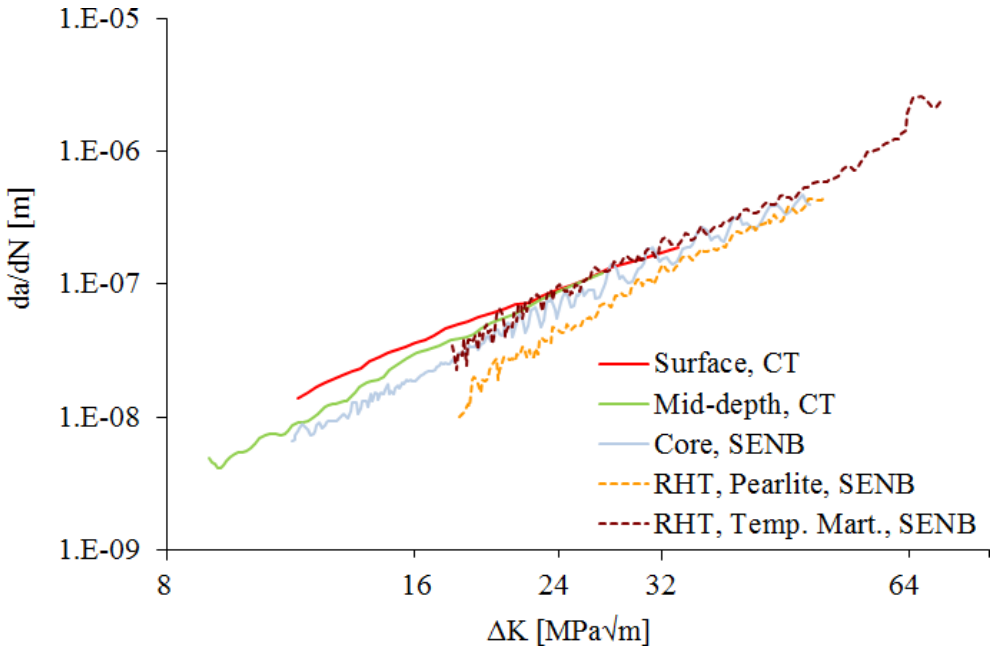

Fig. 12. FCG behavior of B bloom specimens in as-received (surface, middle, and core regions) and RHT (pearlite and tempered martensite) conditions. Plot of K-increasing tests. SENB or CT samples.

Rotating bending fatigue tests were performed on the B and C bloom specimens, the former both in the original and RHT conditions. The specimens were obtained from the surface and core bloom depth, at about 140 and 560 mm, respectively. The test results are listed in Tab. III. The fatigue strength at 4.2 million cycles of the surface specimens is better than the core ones, both in the as-received and RHT conditions. The RHT B bloom samples have an endurance limit about 20% larger than the as-received ones at the same depth.

Tab. III. Fatigue strength at 4.2 million cycles of B (both in the original and re-heat-treated conditions) and C bloom specimens, surface, and core positions.

Survival probability	ISO 1.2738 - B Bloom				C Bloom	
	AR		RHT		AR	
	Core [MPa]	Surface [MPa]	Core [MPa]	Surface [MPa]	Core [MPa]	Surface [MPa]
50%	493±19	559±17	608±24	700±5	565±7	629±15

3.4 Toughness and fractography

The plane-strain fracture surfaces of the B bloom specimens, do not show appreciable crack-tip blunting, and exhibit different rupture modes, as a function of the bloom depth, Fig. 13. The fracture appearance of surface specimens is generally brittle with mixed intergranular and quasi-cleavage pattern. The propagation of the fracture along the grain boundaries may be related to a weakening effect due to elemental segregations, probably caused by the long duration of the steelwork heat treatments. Where the grain boundaries are not in a favorable position and orientation in respect to the overall fracture plane, transgranular fracture of some grains occurs by cleavage. The size of the intergranular fracture facets and of the uninterrupted cleavage regions upon the fracture surfaces is in reasonable agreement with the above-mentioned PAG measurements, suggesting that the intergranular fracture occurs along the previous austenite grain boundaries. Small ductile areas are generally found in the transition zone among different cleavage regions or cleavage and intergranular ones.

The integranular fracture area fraction steeply decreases with depth, being replaced by quasi-cleavage fracture, that is prevalent at intermediate depths (approximately from 230 to 395 mm), where the microstructure is mainly bainite. Cleavage is gradually substituted by ductile areas at increasing depth from 230 to core (645 mm), that may cause the moderate K_{Ic} increase toward the core. The tensile fracture surfaces of A and B bloom samples are always ductile.

Depth	K_{Ic} fracture surface
Surface (a)	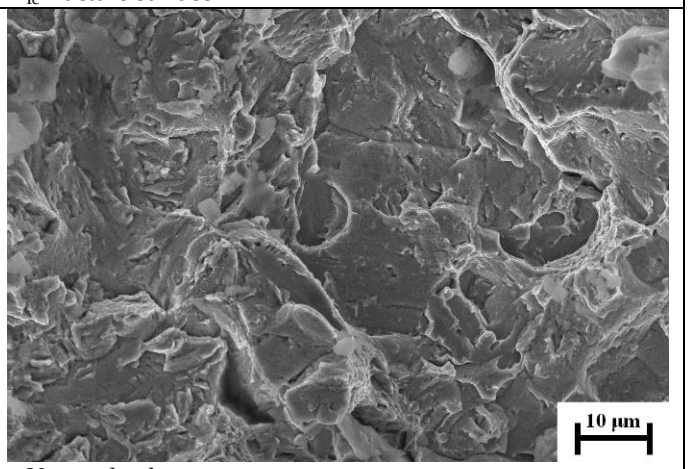 ~60 mm depth
Mid-depth (b)	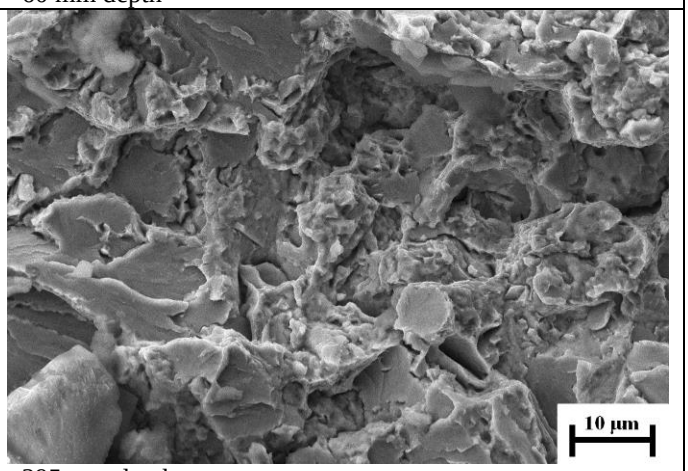 ~395 mm depth
Core (c)	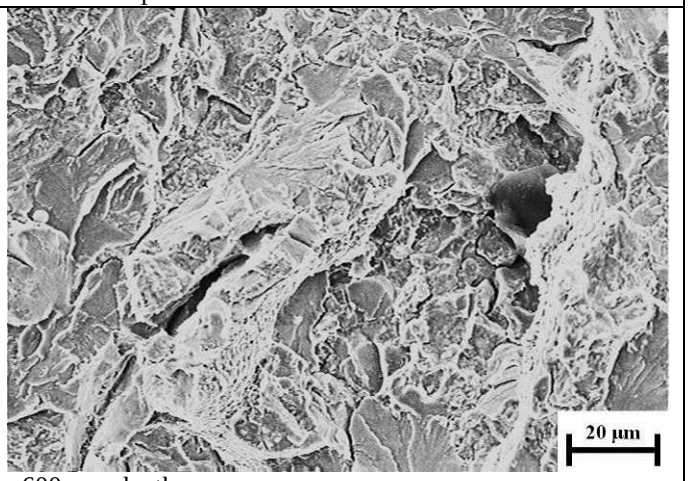 ~600 mm depth

Fig. 13. K_{Ic} fracture surface of B bloom steel specimens in surface, middle, and core regions. Mixed intergranular and cleavage (a) and quasi-cleavage regions (b,c).

The plane-strain fracture surfaces of the RHT B bloom samples, Fig. 14, show mixed intergranular and quasi-cleavage fracture, like that observed in the as-received bloom surface ones, probably due to the similar overall microstructure (tempered martensite).

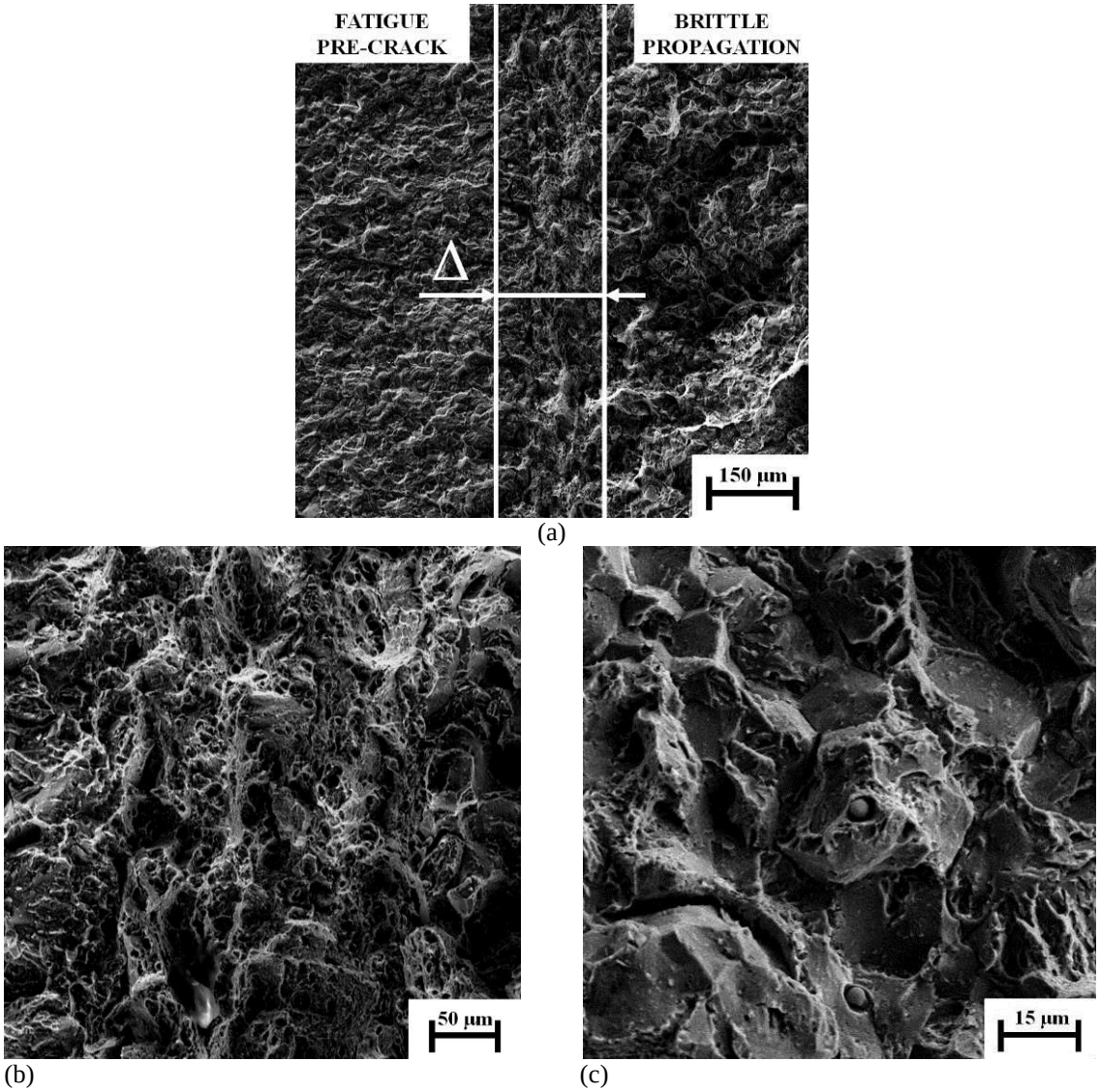

Fig. 14. Plane-strain fracture surfaces of the RHT B bloom specimens. (a) Region at the pre-crack tip, (b) magnification of the plastic tearing region (Δ); (c) brittle propagation of fracture by mixed intergranular and cleavage pattern.

Moreover, they also show a plastic tearing region (Δ) at the pre-crack tip, that is absent in all others bloom materials, Fig. 15. The extension of this region can explain the higher fracture toughness obtained from the RHT samples, in

respect to the original bloom steel specimens, and is probably the cause of the large K_{Ic} data scattering of the RHT samples (e.g., K_{Ic} values of 63 and 103 MPa√m were obtained from samples with Δ equal to about 15 and 50 μm, respectively). In the whole bloom depth, the C steel plane-strain fracture surfaces exhibit a brittle appearance with prevalent large cleavage facets and some intergranular regions, Fig. 15. A similar morphology also occurs on the fracture surfaces of the core tensile samples, whereas some ductile areas appear in mid-depth tensile samples and become prevalent in surface ones, Fig. 16.

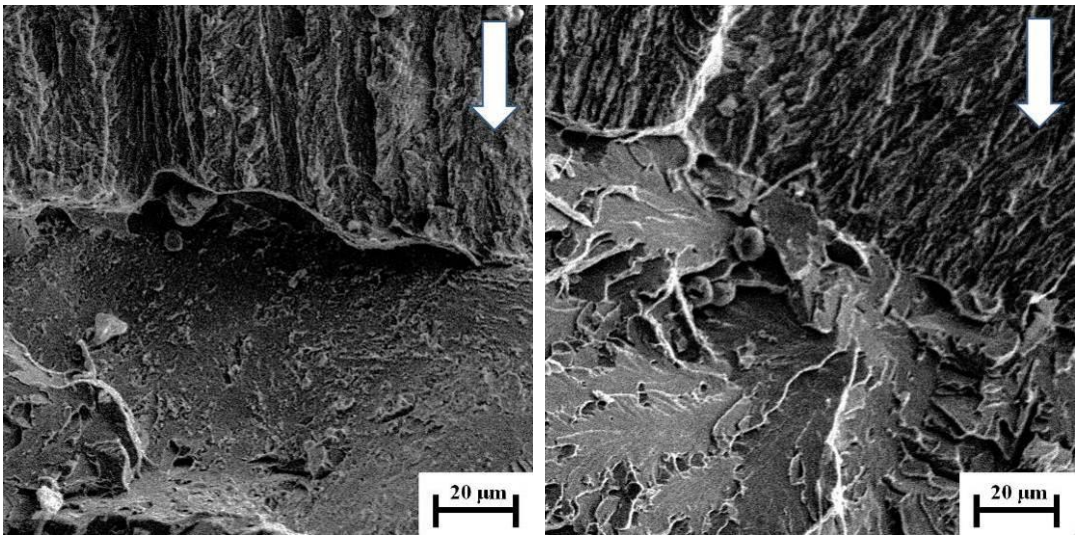

(a) (b)

Fig. 15. Plane-strain fracture surfaces of the C bloom specimens at the onset of crack propagation; surface (a) and core (b) samples. Arrows indicate crack propagation direction.

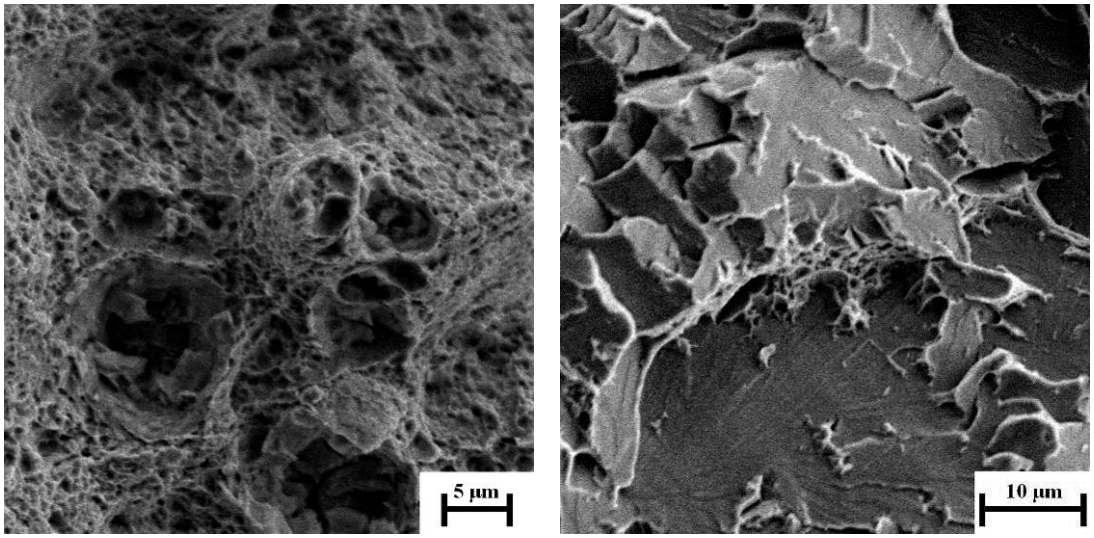

(a) (b)

Fig. 16. Tensile fracture surfaces of the C bloom specimens; (a) ductile fracture of the surface samples; (b) cleavage fracture of the core samples.

The plane-strain fracture surfaces of the as-received D bloom samples show mainly cleavage facets, with some microscopically ductile intergranular ruptures, Fig. 17; the latter are prevalent in tensile fracture surfaces of the as-received and aged samples, Fig. 18a, whereas the RHT and aged tensile samples show completely ductile fracture surfaces, Fig. 18b. Also in this case, the intergranular fracture may be caused by elemental segregations at PAG boundaries.

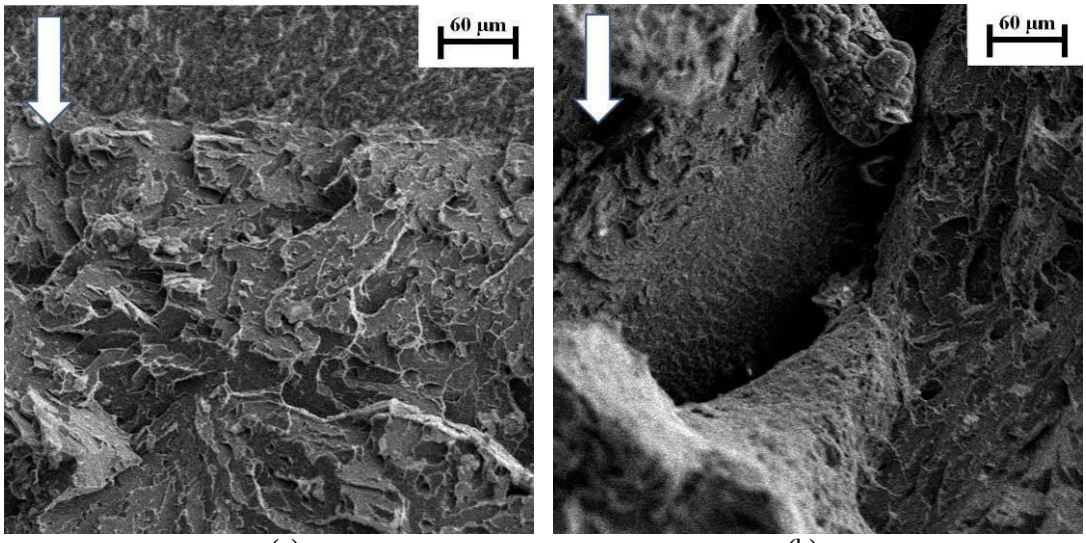

(a) (b)

Fig. 17. Plane-strain fracture surfaces of the D bloom samples at the onset of crack propagation (a) and in the unstable propagation region (b). Overall, the fracture surface exhibits cleavage facets (a), even if an intergranular fracture (b) can sometimes occur. Arrows indicate crack propagation direction.

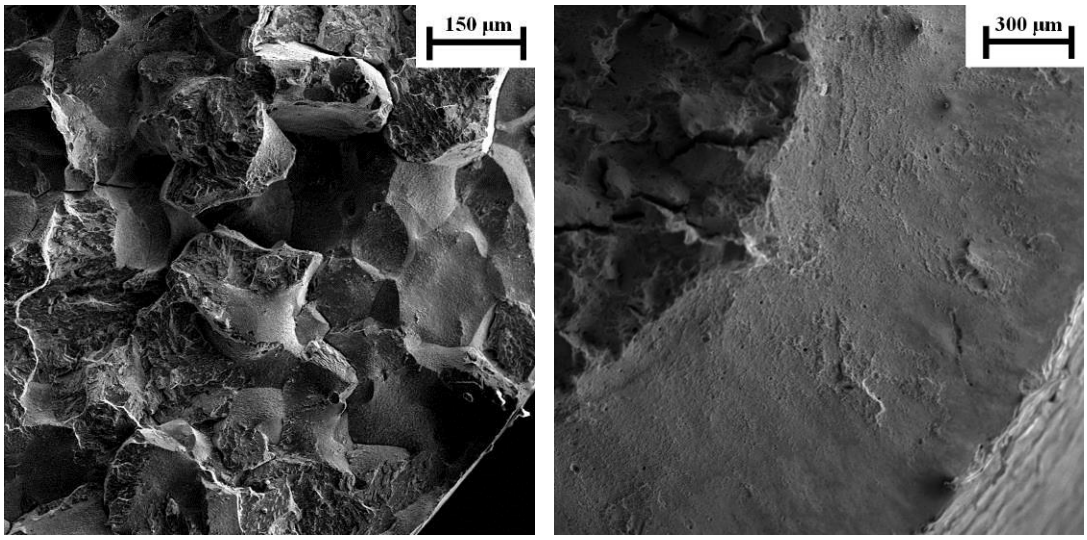

(a) (b)

Fig. 18. Tensile fracture surfaces of the D bloom samples. (a) Intergranular fracture of the as-received sample aged at 550 °C for 2.5 h; (b) ductile fracture of the RHT sample aged at 550 °C for 2.5 h.

4. Discussion

The examined ISO 1.2738 steel blooms show different microstructures from surface to core, and blooms obtained from different steelmaking practices may show significant differences in the mechanical properties, PAG size and in the microstructural segregation, presumably due to different heat treatments and forging schedules performed in steelworks. The metallographic observations show mixed microstructures through the A and B blooms: tempered martensite is present close to the surface, upper and lower bainite (affected by tempering) are the prevalent constituents in the intermediate regions, whereas pearlite gradually appears at higher depths and becomes the main constituent at core (Figs. 4, 5). The microstructure of the microalloyed steel bloom is overall more homogeneous than that of the ISO 1.2738 grade A and B blooms: tempered bainite is present in the whole bloom thickness, with tempered martensite being present only in the surface regions. The microstructure of the examined position inside the E steel bloom consists of tempered bainite (Fig. 5).

Consistently with the microstructural observations, the hardness and tensile properties of the ISO 1.2738 grade A and B steels are significantly influenced by the distance from the bloom surface (e.g., for the B bloom, the UTS and YS are about 1100 and 950 MPa close to the surface, while they are 950 and 660 MPa at core, respectively), whereas the microalloyed C steel bloom exhibits somewhat higher strength and remarkably more homogeneous tensile properties (YS, UTS and hardness mean values are 989 ± 17 MPa, 1144 ± 21 MPa and 375 ± 7 HV 100).

The fracture toughness of the examined ISO 1.2738 grade B blooms is really low (mean value 40 MPa√m) for quenched and tempered steels, considering the achieved UTS. The plain-strain fracture in the as-received specimens prevalently occurs by decohesion along either grain boundaries or cleavage planes, meaning that the brittle-to-ductile transition is not overcome. The moderate increase in fracture toughness with the bloom depth may be attributed to the appearance of some ductile areas with shallow dimples, that are absent close to the surface.

By comparison, the fracture toughness of RHT B specimens is remarkably higher (from 63 to 103 MPa√m), even at somewhat higher strength levels. Thus, the observed low toughness of the as-received specimens must be attributed to the mixed microstructures caused by the steelwork heat treatment, and in general to the large size of the blooms, as already signaled elsewhere [21].

In the RHT B specimens, the fracture is mainly intergranular with a significant fraction of quasi-cleavage. Their fracture toughness results present a large data scattering that may be attributed to the ductile region at the pre-crack tip. It should be noticed that the microstructure features of the RHT samples and of the more superficial bloom samples are similar within the limits of differences amenable by optical metallography (tempered martensite); thus, the difference in fracture toughness and resilience should be attributed to microstructural differences on a sub-micron scale, for example to grain boundary segregation or precipitation phenomena occurring during the long bloom tempering stages.

The fracture toughness of microalloyed C bloom (about 54 MPa√m at surface and 44 MPa√m at middle depth and core) is somewhat larger than that achieved by the A and B ones, and still much lower than the K_{Ic} of individually quenched and tempered RHT B bloom samples, despite the completely brittle plane-strain fracture surfaces of the C bloom specimens (opposed to the partially ductile of the B and C ones). The fracture toughness of C bloom decreases between the surface and middle depth positions probably due to the reduction of the amount of tempered martensite with increasing depth. Moreover, the C bloom shows a transition toward a more brittle fracture mode at core, as evidenced by the variation of both the tensile reductions of area ratios (with necking being substantially

absent at core) and the tensile fracture surfaces (being almost completely brittle at core); no such transition occurs in the A and B bloom specimens, their room temperature tensile fracture behavior being everywhere ductile.

The as-received D steel exhibits the largest fracture toughness (70 MPa√m) among the examined blooms, together with acceptable strength and hardness. It is uncertain whether these properties are homogeneous since no core material was examined, even if previous quenching calculations [22] support such hypothesis.

The substantially asymptotic age hardening of the D bloom specimen at the examined aging temperatures (Fig. 7), for times up to 8 h, may allow to obtain homogeneous results also in the aging of molds with large cross-section, even though the actual effective aging duration is different from surface to core. Nevertheless, the aging treatment generally causes a relevant toughness reduction, so it may not always be advantageous.

From the fatigue crack growth test results, it is understood that almost all as-received bloom specimens exhibit similar fatigue crack growth resistance and fatigue thresholds, despite the different microstructures (Figs. 11 and 12). The overall FCG rate of the B bloom specimens generally decreases (for a fixed SIF cycle, or ΔK) from surface to core. This result can be compared to the fatigue strength at $4.2 \cdot 10^6$ cycles of smooth rotating bending specimens cut from the same bloom, that generally decreases from surface to core. In the Paris law region, the FCG behavior of the B bloom surface material, that consists mainly of tempered martensite, is very similar to that of the RHT tempered martensite sample, despite the much lower fracture toughness (K_{Ic} = 35 vs. ~80 MPa√m) of the former. In the bloom core, the pearlitic microstructure has a FCG rate higher than the RHT pearlite samples. By comparing the FCG results of the as-received and ISO 1.2738 RHT bloom samples, it is apparent that, at ΔK values larger than 20 MPa√m the tempered martensite and the pearlite can be regarded as an upper and a lower boundary, respectively, for the FCG rate of the varying microstructures inside a pre-hardened bloom.

Therefore, the FCG rate behavior of the B bloom steel is influenced by the micro-constituents, and pearlite is more beneficial to the FCG performance than tempered martensite (even if the opposite occurs for the fracture toughness values), since the former shows a FCG rate ~30% lower than the latter in the 20 to 50 MPa√m ΔK range. Since the fatigue life of a smooth specimen first consists of short-crack nucleation and early growth and then of long-crack growth (only the latter being described by the Paris curve), it is concluded that the superior performance of the surface samples in the rotating bending fatigue tests, as opposed to the core ones, may stem from a longer time for crack nucleation, or lower rate of short-crack growth. Results concerning the C bloom show that its rotating bending fatigue limit is larger than that obtained by B bloom,, and that its FCG rate is smaller than that of B bloom up to 20

MPa√m, but higher thereafter (since the overall Paris slope of C bloom specimens is larger). In this case, the superior performance of the surface C bloom material in the rotating bending fatigue test can be justified by the smaller FCG rate observed the smallest ΔK values.

The room temperature Charpy impact energy measured on the B bloom, both in surface and core regions, is very low, about 10 J. The re-heat-treatments have only a slight positive effect on the steel Charpy impact energy that increases up to 20 J. The low absorbed impact energy values and the high brittle-to-ductile transition temperatures measured on B bloom are consistent with the K_{Ic} results and show that, in consideration of the usual (inhomogeneous) service temperatures of plastic molds, this steel bloom is mostly used in the brittle range of its brittle-to-ductile transition curve. Nevertheless, upon considering the Charpy tests carried out at 175 °C, the A bloom, obtained from a different manufacturer, has shown evidences of a remarkably higher impact energy than B bloom, despite its microstructure was coarser and less homogeneous and exhibited a larger amount of pearlite, in respect to B bloom. Reasons for this difference are not clear and require further investigations.

The rotating bending fatigue strength of B and C blooms (at 4.2 million cycles) is better in surface samples than core ones, the former both in the as-received and RHT conditions (Tab. III). The specimens cut from the microalloyed C steel bloom have a higher fatigue strength than the B specimens, for the same bloom depth. The endurance limit of the two bloom steels apparently do not scale with the other mechanical properties, such as fracture toughness or steel tensile strength. The re-heat-treatment increases of about 20 % the fatigue strength, although keeping decreasing values with the bloom depth, as it was for the as-received condition. The reasons of the latter fact are still object of discussion.

Overall, the C steel appears competitive in respect to the traditionally ISO 1.2738 steel, but not definitely superior. Among the presently considered steels, D steel shows the best combination of toughness and strength, but a definitive conclusion will only be obtained by testing a set of specimens representative of an entire bloom, in order to confirm the hypothesized bloom homogeneity.

5. Conclusions

Mixed microstructures occur throughout the quenched and tempered A, B, and C blooms, thus the hardness and the tensile properties significantly vary inside the blooms, even if the variation is smaller for the microalloyed C one.

The fracture toughness values of the quenched and tempered steel blooms are low (in the 35-55 MPa√m range), considering the achieved ultimate tensile strength (in the 900-1150 MPa range). By comparison, the individually re-heat-treated quenched and tempered samples exhibit a mean fracture toughness of 80 MPa√m.

The precipitation hardenable D bloom, in the examined regions and in the as-received condition, exhibits a bainitic microstructure with higher fracture toughness (70 MPa√m) in respect to the quenched and tempered steel bloom, but it decreases after aging (44 MPa√m).

The fatigue crack growth behavior of the B and C blooms is quite similar, with the former having a slightly higher Paris slope; the behavior of B steel is not significantly modified after the quench and tempering re-heat-treatment. The rotating bending fatigue strength of the B and C steels scales with the tensile strength, with the C bloom exhibiting the highest values. The re-heat-treatment improves of about 25% the fatigue strength of the B bloom.

The present research demonstrates that the fracture toughness is the most critical property for the examined steels and their usual applications, as dictated by the bloom size and by the commonly employed production cycle of large plastic molds; it also demonstrates that heat treatments performed on the massive blocks are not able to fully exploit the capability of the steel. Therefore, the verification of the mold design against the brittle fracture risk, by using the fracture mechanics approach and taking into account the actual metallurgical conditions, should be recommended.

References

[1] ISO 4957:1999, Tool Steels, International Organization for Standardization, Geneve, Switzerland, 1999.

[2] D. Firrao, P. Matteis, G. Scavino, G. Ubertalli, M.G. Ienco, M.R. Pinasco, E. Stagno, R. Gerosa, B. Rivolta, A. Silvestri, G. Silva, A. Ghidini, Mater. Sci. Eng. A 468–470 (2007) 193–200.

[3] D. Firrao, R. Gerosa, A. Ghidini, P. Matteis, G.M.M. Mortarino, M.R. Pinasco, B. Rivolta, G. Silva, E. Stagno, Int. J. Fatigue 29 (2007) 1880–1884.

[4] T. Gladman, The Physical Metallurgy of Microalloyed Steels, The Institute of Materials, University Press, Cambridge, 2002.

[5] A.M. Bayer, T. Basco, L.R. Walton, Wrought tool steels, properties and selection: irons, steels and high performance alloys, in: Metals Handbook tenth ed., Vol. 1, ASM International, Materials Park, OH, 1990, pp. 757–779.

[6] G.A. Roberts, R.A. Cary, Tool Steels, fourth ed., ASM International, Materials Park, OH, 1980.

[7] T. Schade, Mold Making Technology Magazine, Oct. 2003.

[8] P.M. Unterweiser, H.E. Boyer, J.J. Kubbs, Heat Treaters's Guide: Standard Practices and Procedures for Steel, ASM International, Materials Park, OH, 2010, pp. 580–588.

[9] C.C. Davis, Metal Handbook, ninth ed., Properties and Selection: Stainless Steels, Tool Materials and Special Purpose Metals, vol. 3, ASM International, Materials Park, OH, 1980, pp. 546–550.

[10] ASTM E112-10, Standard Test Methods for Determining Average Grain Size, ASTM International, West Conshohocken, PA, 2010. [11] S. Bechet, L. Beaujard, Rev. Met. 52 (1955) 836–837.

[12] ASTM E1820-11, Standard Test Method for Measurement of Fracture Toughness, ASTM International, West Conshohocken, PA, 2011.

[13] ASTM E399-09, Standard Test Method for Plane-Strain Fracture Toughness of Metallic Materials, ASTM International, West Conshohocken, PA, 2009.

[14] ISO 12108:2002, Metallic materials – Fatigue testing by Fatigue Crack Growth Method, International Organization for Standardization, Geneve, Switzerland, 2002.

[15] ASTM E647-11, Standard Test Method for Measurement of Fatigue Crack Growth Rates, ASTM International, West Conshohocken, PA, 2011.

[16] D. Firrao, P. Matteis, P. Russo Spena, M.R. Pinasco, G. Pellati, B. Rivolta, R. Gerosa, A. Silvestri, E.M. Tata, R. Montanari, A. Ghidini, Proceedings of the 32nd Convegno Nazionale AIM, Ferrara, Italy, 2008, pp. 1–11. [17] G.K. Narita, Trans. Iron Steel Inst. Jpn. 15 (1975) 152–158.

[18] P. Matteis, Tenacita' a Frattura di Stampi per Materie Plastiche: Dipendenza dal Ciclo Produttivo, dal Trattamento Termico e dalla Microstruttura, Ph.D. Thesis, Politecnico di Torino, 2006, p. 42.

[19] M.R. Pinasco, M. Fabbreschi, D. Firrao, R. Gerosa, A. Ghidini, P. Matteis, B. Rivolta, Proceedings of the Materials Science & Technology 2008 Conference and Exhibition, Pittsburgh, USA, 2008, pp. 1916–1935.

[20] D. Firrao, P. Matteis, G.M.M. Mortarino, P. Russo Spena, M.G. Ienco, G. Pellati, M.R. Pinasco, R. Gerosa, G. Silva, B. Rivolta, E.M. Tata, R. Montanari, Metall. Ital. 4 (2009) 1–10.

[21] D. Firrao, P. Matteis, Frattura ed Integrita' Strutturale 18 (2011) 54–68.

[22] D. Firrao, M. Chiarbonello, P. Matteis, G.M.M. Mortarino, P. Russo Spena, G. Scavino, G. Ubertalli, M.G. Ienco, G. Pellati, M.R. Pinasco, E. Stagno, R. Gerosa, B. Rivolta, A. Tavasci, E.M. Tata, R. Montanari, A. Silvestri, G. Silva, S. Missori, A. Ghidini, Proceedings of the TMS Annual Meeting 2007, Orlando, USA, 2007, pp. 69–78.